Article

Cortical ensembles orchestrate social competition through hypothalamic outputs

https://doi.org/10.1038/s41586-022-04507-5

Received: 17 October 2020

Accepted: 2 February 2022

Published online: 16 March 2022

Check for updates

Nancy Padilla-Coreano[1,12], Kanha Batra[1,2,12], Makenzie Patarino[1], Zexin Chen[3], Rachel R. Rock[4], Ruihan Zhang[4], Sébastien B. Hausmann[1,5], Javier C. Weddington[4], Reesha Patel[1], Yu E. Zhang[6], Hao-Shu Fang[3], Srishti Mishra[1], Deryn O. LeDuke[1], Jasmin Revanna[1], Hao Li[1], Matilde Borio[1], Rachelle Pamintuan[1], Aneesh Bal[1], Laurel R. Keyes[1,7], Avraham Libster[1], Romy Wichmann[1], Fergil Mills[1], Felix H. Taschbach[1,8], Gillian A. Matthews[1], James P. Curley[9], Ila R. Fiete[10], Cewu Lu[3,11] ✉ & Kay M. Tye[1,7] ✉

Most social species self-organize into dominance hierarchies[1,2], which decreases aggression and conserves energy[3,4], but it is not clear how individuals know their social rank. We have only begun to learn how the brain represents social rank[5–9] and guides behaviour on the basis of this representation. The medial prefrontal cortex (mPFC) is involved in social dominance in rodents[7,8] and humans[10,11]. Yet, precisely how the mPFC encodes relative social rank and which circuits mediate this computation is not known. We developed a social competition assay in which mice compete for rewards, as well as a computer vision tool (AlphaTracker) to track multiple, unmarked animals. A hidden Markov model combined with generalized linear models was able to decode social competition behaviour from mPFC ensemble activity. Population dynamics in the mPFC predicted social rank and competitive success. Finally, we demonstrate that mPFC cells that project to the lateral hypothalamus promote dominance behaviour during reward competition. Thus, we reveal a cortico-hypothalamic circuit by which the mPFC exerts top-down modulation of social dominance.

The mPFC is best known for its role in higher cognitive functions, with theoretical emphasis on mPFC integration of sensory and limbic information to flexibly guide behaviour on the basis of task rules[12]. Notably, mPFC circuitry has also been implicated in social cognition, social memory and dominance[7,8,11,13,14]. We hypothesized that mPFC neurons encode social rank and are part of top-down circuits to guide behaviour on the basis of social rank[15].

We designed a reward competition assay wherein mice that were linearly ranked among their cage mates competed for a liquid reward delivered during a tone. This task design optimized rigorous statistical examination of ethologically relevant behaviours in a trial structure (Fig. 1a). We considered relative social ranks within each competing pair, enabling a within-subject comparison for intermediate-ranked animals. After individually learning that the tone predicted reward delivery (Extended Data Fig. 1a), mice competed for rewards with a cage mate. Dominant mice, as defined by the tube test[8], obtained more rewards, spent more time at the reward port and were more successful at displacing competitors (Fig. 1b, c and Extended Data Fig. 1).

To automatically track the behaviour of multiple, unmarked mice, we developed AlphaTracker, a deep-learning computer vision tool that combines two neural networks, one to create a bounding box for each subject, and another for pose estimation to detect multiple, unmarked animals (Fig. 1d, e). AlphaTracker also applies another algorithm to track animal identity across frames considering animal positions from the previous frame (Fig. 1d; see Supplementary Methods). The performance of AlphaTracker surpasses human accuracy when tracking two or four mice (Extended Data Fig. 2) and includes unsupervised clustering of high-dimensional tracking output data to aid in the identification of novel behavioural motifs (Extended Data Fig. 3 and Supplementary Video 1).

mPFC neurons encode competition behaviour

To investigate whether mPFC neurons encode competition behaviours, we used wireless head-mounted devices to record cellular-resolution activity during the social competition (Fig. 1f, g and Extended Data Figs. 4 and 5a–g). After AlphaTracker facilitated identification of nine different behavioural labels (Fig. 1f and Extended Data Fig. 5h, i), we investigated whether the mPFC predicted specific behavioural outputs. Given the ability of mPFC neurons to be selective for different stimulus features under different contexts[16], we posited that mPFC neural activity could be dynamic, and that representations may be

[1]Salk Institute for Biological Studies, La Jolla, CA, USA. [2]Department of Electrical and Computer Engineering, University of California San Diego, La Jolla, CA, USA. [3]Department of Computer Science, School of Electronics, Information and Electrical Engineering, Shanghai Jiao Tong University, Shanghai, China. [4]The Picower Institute for Learning and Memory, Department of Brain and Cognitive Sciences, Massachusetts Institute of Technology, Cambridge, MA, USA. [5]Swiss Federal Institute of Technology (EPFL), Lausanne, Switzerland. [6]Neurobiology Section, Center for Neural Circuits and Behavior, and Department of Neurosciences, University of California San Diego, La Jolla, CA, USA. [7]Howard Hughes Medical Institute, Salk Institute for Biological Studies, La Jolla, CA, USA. [8]Neurobiology Section, Division of Biological Sciences, University of California San Diego, La Jolla, CA, USA. [9]Department of Psychology, University of Texas at Austin, Austin, TX, USA. [10]McGovern Institute for Brain Research, Department of Brain and Cognitive Sciences, Massachusetts Institute of Technology, Cambridge, MA, USA. [11]Shanghai Artificial Intelligence Laboratory, Shanghai, China. [12]These authors contributed equally: Nancy Padilla-Coreano, Kanha Batra. ✉e-mail: lucewu@sjtu.edu.cn; tye@salk.edu

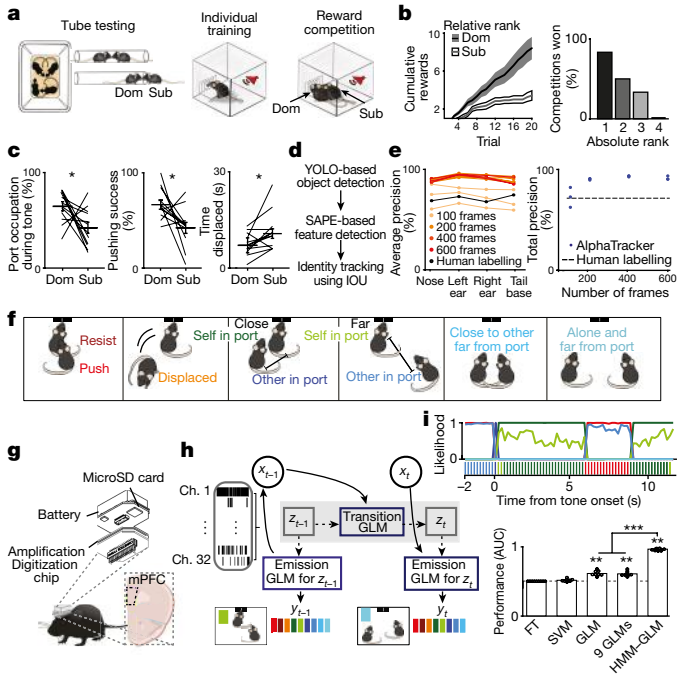

Fig. 1 | Novel social dominance assay and deep learning tool for tracking multiple animals. a, Reward competition behavioural paradigm. **b**, Mice with higher relative ranks (dominant (Dom)) collected more rewards than relative subordinates (Sub) when competing in dyads ($n = 12$ dyads; sign rank test on total rewards, $P = 0.008$). Left, cumulative rewards across trials. Right, percentage of competitions won by absolute rank ($n = 6$ competitions per rank). **c**, Port occupation, pushing success (pushing that resulted in displacement of competitor) and time displaced from port differed by relative rank ($n = 12$ dyads; sign rank test, occupation $P = 0.04$; pushing success $P = 0.02$; displaced $P = 0.016$). **d**, Architecture of AlphaTracker, which combines two convolutional neural networks (YOLO, you only look once; SAPE, single-animal pose estimation, which is a squeeze-and-excitation network) and intersection over union (IOU) for identity tracking. **e**, AlphaTracker precision for tracking two unmarked, near-identical mice is higher than human precision separated by body parts (left) or total (right; average precision across body parts; $n = 3$ subsampled replicates). **f**, Social competition behavioural labels used for decoder models. **g**, Wireless device to record neural activity from the mPFC ($n = 965$ trials from 32 sessions from 13 mice). Image modified from SpikeGadgets. **h**, Architecture of the HMM–GLM model to describe the relationship between neural activity and behavioural states. Hidden states are shown on the grey background. Ch, channel; x, mPFC activity; y, behaviour label; z, hidden state. **i**, Top, example trial with real behavioural labels and prediction for HMM–GLM six-state model (colours from **f**). Bottom, performance across models based on area under the receiver operating curve (AUC; $n = 9$ behaviours; Kruskal–Wallis test $P = 6.7 \times 10^{-8}$; model versus chance sign test $P = 0.004$ for six-state HMM–GLM, 9 GLMs and GLM; Wilcoxon rank sum HMM–GLM versus GLM $P = 4 \times 10^{-5}$, HMM–GLM versus 9 GLMs $P = 4 \times 10^{-5}$, GLM versus 9 GLMs $P = 0.54$). FT, frequency of behaviours table. Data are presented as mean values ± s.e.m. $^*P < 0.05$, $^{**}P < 0.01$, $^{***}P < 0.001$.

hierarchical, and influenced by internal hidden states. We turned to an unsupervised method to identify hidden states by combining a hidden Markov model (HMM) with generalized linear models (GLMs)[17,18] and adapted it to use mPFC neural activity to predict behaviour. In our HMM–GLM model, one set of multinomial GLMs predicts the transition probabilities between hidden states, and each hidden state is paired with another multinomial GLM that describes the relationship between neural activity and behaviour (Fig. 1h).

An HMM–GLM model with six hidden states decoded behavioural labels from neural activity with superior cross-validated performance compared with that of static models (Fig. 1i, Extended Data Fig. 5j and Supplementary Video 2). The model performed equally well when training for one relative rank and testing on the other (Extended Data Fig. 5k, l), suggesting that mPFC encoding of social competition behaviour is generalizable across relative ranks. Given this finding, we then considered whether there is a stable and simple encoding of rank in mPFC neural representations, and whether these variables could themselves predict behaviour.

mPFC reflects rank and winning

We next investigated whether mPFC neural activity could be used to decode relative social rank, and whether the neural representation of relative social rank is triggered by discrete task-relevant events (cued competition trials or port entries) or stably represented throughout the task. To visualize population activity, we plotted the population activity vector for task-relevant events (Extended Data Fig. 6a and Supplementary Video 3) in a lower-dimensional firing-rate space using principal component analysis. Neural trajectories during the cue and port entries of the self or other (competitor) for win or lose trials occupied segregated neural activity subspaces even before the cue onset, suggesting separable brain states preceding each trial (Fig. 2a and Extended Data Fig. 6), consistent with primate studies[19]. Relative subordinates had longer neural trajectories compared with those of relative dominants (Fig. 2b and Extended Data Fig. 6b–f). Indeed, our analyses revealed larger firing rate variance, but not faster firing rate changes, for relative subordinate mice (Fig. 2b and Extended Data Fig. 6c). We ruled out the possible contributions of potential confounds (for example, subject location, distance to reward port and identity) to the differences in neural trajectories across ranks (Extended Data Fig. 7).

mPFC predicts future wins

To directly test the hypothesis that the mPFC encodes relative rank and competitive success at the population level, we trained a support vector machine (SVM) classifier to decode these binary states from single-trial data (Extended Data Fig. 8a). An SVM was able to decode both competitive success and relative rank—even before cue onset (Fig. 2c and Extended Data Fig. 8b–e), consistent with the notion that state differences in the mPFC correlate with future winning[7]. Social rank was more accurately decoded than competition outcome from mPFC neural activity (Fig. 2c), perhaps reflecting the relative stability of rank versus competitive success. Although our data are consistent with the idea of a 'winning effect' or a 'losing streak'[7,20], the decoding accuracy across the trial was consistently above chance. PFC neural activity could predict whether the next trial would be a win or a loss ~30 s before the competition trial began, providing cellular evidence supporting the psychological concept of 'a winning mindset'.

Notably, we can decode the absolute social rank of individuals from mPFC activity, even when they are alone (Extended Data Fig. 8f–h). To visualize differences between tone responses to the reward while alone versus in competition, we plotted the neural trajectories across tasks in the same subspace of the principal component analysis (Fig. 2d). Subordinate mice (rank 4) had larger changes induced by competition with longer tone trajectory lengths during competition (Fig. 2e). By contrast, dominants (rank 1) showed the smallest differences between the alone and competition state. To confirm that population dynamics differed between receiving the reward alone versus winning, we recorded the same neurons while animals performed the reward task alone versus in competition and found that an SVM could decode trial type from mPFC population dynamics (Extended Data Fig. 8i, j). Notably, relative rank could be predicted in intermediate-ranking animals (Extended Data Fig 8e). However, we cannot rule out the possibility that the representation may reflect social identity and the associated social history with that individual rather than relative rank alone; indeed, it is yet unclear whether the brain is capable of separably representing

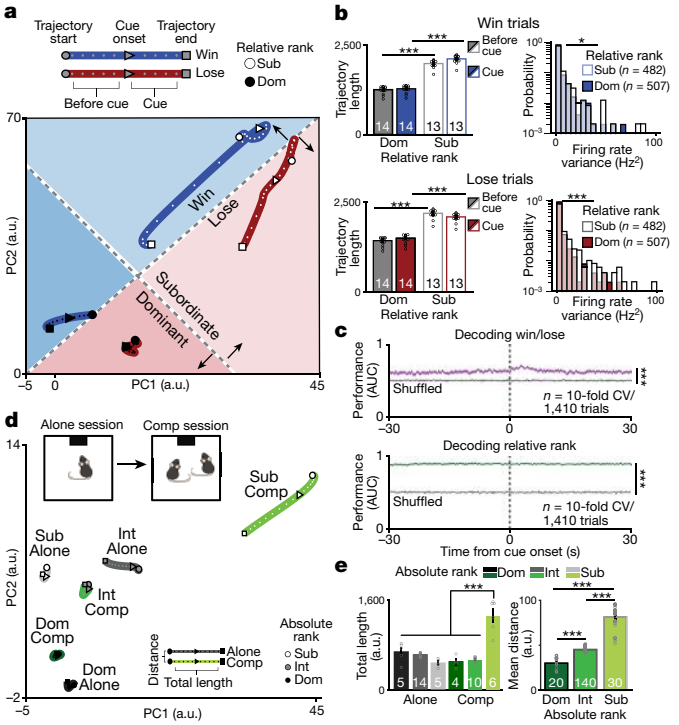

Fig. 2 | Social rank and competitive success is decoded by mPFC population dynamics. a, Neural trajectories of mPFC firing rate differ by relative rank during the tone presentation for win and lose trials in a lower-dimensional common principal component (PC) subspace (trajectories include a total of 20 mice; 27 sessions; dominants, $n = 507$ cells; subordinates, $n = 482$ cells). a.u., arbitrary units. **b**, Neural trajectory lengths for win (top; two-way repeated measures analysis of variance (ANOVA) effects of relative rank $F_{1,25} = 1{,}090$, $P = 2 \times 10^{-16}$ and interaction $F_{1,25} = 1{,}660$, $P = 3 \times 10^{-14}$) and lose (bottom; two-way repeated measures ANOVA effect of relative rank $F_{1,25} = 883$, $P = 9 \times 10^{-16}$ and interaction $F_{1,25} = 2{,}995$, $P = 9 \times 10^{-16}$) trials. Firing rate variance is higher for relative subordinates (number of neurons indicated in plots; top, win trials: Kolmogorov–Smirnov test $P = 0.01$, Wilcoxon rank sum $P = 0.19$; bottom, lose trials: Kolmogorov–Smirnov test $P = 5 \times 10^{-7}$, Wilcoxon rank sum $P = 2 \times 10^{-9}$). Light blue and pink indicate overlapping bars. **c**, SVM performance is higher than chance for decoding competitive success (top) and relative rank (bottom) (grey: shuffled data performance; Wilcoxon rank sum: competitive success $P = 2 \times 10^{-4}$, relative rank $P = 2 \times 10^{-4}$; competitive success versus relative rank $P = 2 \times 10^{-4}$). CV, cross-validation. **d**, Neural trajectories of mPFC population firing rate by absolute rank (dominant = rank 1; intermediates (Int) = ranks 2 and 3; subordinate = rank 4) when performing the reward task alone versus in competition (Comp) in a lower-dimensional common PC subspace (neurons in alone session: dominant = 111, intermediate = 259, subordinate = 140; competition: dominant = 309, intermediate = 359, subordinate = 330). **e**, Left, trajectory during the tone is higher for subordinates during competition (two-way ANOVA main effect of rank $F_{2,38} = 30.4$, $P = 1 \times 10^{-8}$, task $F_{1,38} = 26.1$, $P = 9 \times 10^{-6}$ and interaction $F_{2,38} = 70.1$, $P = 1 \times 10^{-13}$). Right, distance between alone and competition tone trajectories increases with rank (n reflects all possible combinations of alone versus competition trajectories; one-way ANOVA main effect of rank $F_{2,187} = 536$, $P = 3 \times 10^{-78}$). Post-hoc comparisons are Bonferroni-corrected t-tests, $^{*}P < 0.05$, $^{***}P < 0.001$. Two-way ANOVAs were for rank and event (baseline versus event) or rank and trial type and sample size indicated in plots. Data are presented as mean ± s.e.m.

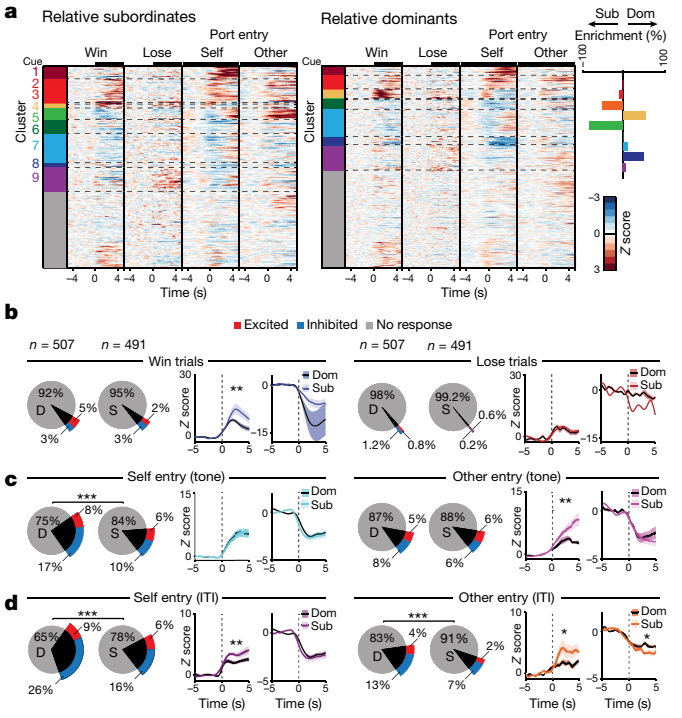

Fig. 3 | Relative dominants have more reward-seeking-behaviour cells whereas subordinates have larger responses to competitor behaviour. a, Left, heatmaps for mPFC firing rate responses to task-relevant events during the reward competition. Colours indicate clusters obtained by hierarchical clustering. Cells included in heatmap have a Z score greater than 2 or less than −1 (dominant $n = 326$; subordinate $n = 305$); clusters with a non-responsive population average are labelled grey. Right, difference between relative dominant and subordinate cells (percentage enrichment) across functional clusters. Black horizontal lines represent the cue. **b**, Left, response magnitude for mPFC cells during win trials differed across relative ranks (D, dominant; S, subordinate; Fisher's exact test, total responsive cells per group $P = 0.30$; Wilcoxon rank sum across groups: excited $P = 0.01$; inhibited $P = 0.06$). Right, number of responsive cells and response magnitude for lose trials did not differ by relative rank (Fisher's exact test, total responsive per group $P = 0.17$; Wilcoxon rank sum: excited $P = 0.62$; inhibited $P = 0.28$). **c**, Left, number of mPFC cells responsive to self tone port entry was higher for relative dominants (Fisher's exact test, total responsive cells per group $P = 0.0003$; Wilcoxon rank sum: excitation $P = 0.28$ and inhibition $P = 0.99$). Right, there was no difference in number of cells responsive to other tone port entry whereas the excitation magnitude was higher for relative subordinates (Fisher's exact test, total responsive cells per group $P = 0.84$; Wilcoxon rank sum: excitation $P = 0.006$, inhibition $P = 0.11$). **d**, Left, relative dominants had more mPFC cells responsive to self port entries during the inter-trial interval (ITI) whereas relative subordinates had larger excitation magnitude (Fisher's exact test, $P = 9.8 \times 10^{-6}$; Wilcoxon rank sum: excitation $P = 0.006$ and inhibition $P = 0.28$). Right, relative dominants had more mPFC cells responsive to other port entries during the inter-trial interval whereas subordinates had larger magnitudes (Fisher's exact test, $P = 0.00019$; Wilcoxon rank sum: excitation $P = 0.015$ and inhibition $P = 0.04$). Recordings were collected from 20 mice; sample indicated in plots is cells. Data are presented as mean ± s.e.m. $^{*}P < 0.05$, $^{**}P < 0.01$, $^{***}P < 0.001$.

rank and identity. Together, these data demonstrate that the mPFC has a dynamic, but consistent, representation of social rank and competitive success despite having multiple, rank-independent hidden states for encoding behaviour during social competition.

Rank-dependent mPFC representations

Given that the mPFC encodes social rank and competitive success, we posited that specific ensembles of cells might encode distinct task-relevant events in a rank-dependent manner to provide a distributed representation of social rank and competitive success. To investigate whether social rank is represented within the mPFC at the single-cell level, we analysed the firing rate of individual mPFC neurons during discrete reward competition events. mPFC single units showed diverse responses to the tone for win-or-lose trials and to port entries performed by self or the other (that is, the competitor) that differed by social rank (Fig. 3a and Extended Data Fig. 9a). We quantified the ensemble sizes and magnitude of responses to the task-relevant events

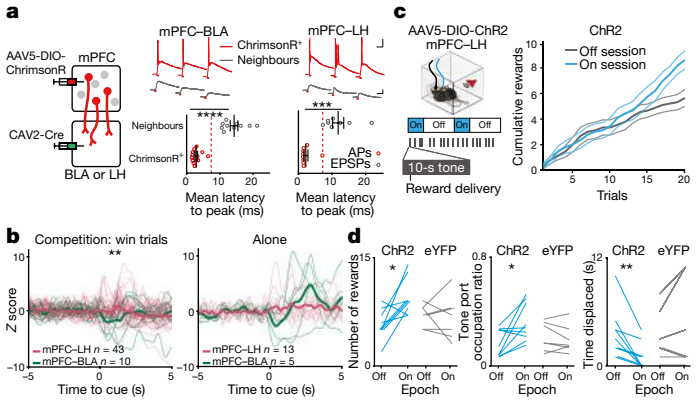

Fig. 4 | mPFC–LH pathway encodes social competition and modulates social dominance behaviour. a, Left, viral strategy to stimulate projectors. Top middle and right, mPFC projector cells (ChrimsonR$^+$; red) and neighbour cells (grey) responding to pulses of red light. Top scale, 40 ms and 20 mV; bottom scale, 40 ms and 4 mV. Bottom middle and right, average photo-latency of action potentials (APs) or excitatory postsynaptic potentials (EPSPs) for mPFC–BLA (left plot) and mPFC–LH (right plot) ChrimsonR$^+$ cells compared to neighbouring cells (mPFC–BLA ChrimsonR$^+$ $n = 12$ versus neighbours $n = 10$; *t*-test, ****$P < 0.0001$; mPFC–LH ChrimsonR$^+$ $n = 9$ versus neighbours $n = 8$; *t*-test, ***$P < 0.001$). Dashed lines indicate photoresponse latency threshold used for phototagging projector. AAV5, adeno-associated virus serotype 5; DIO, double-floxed inverted open reading frame. **b**, Left, firing rate of mPFC–LH is higher than that of mPFC–BLA during the reward delivery (0–2 s) in win trials (mPFC–BLA $n = 10$ neurons, mPFC–LH $n = 42$ neurons, Wilcoxon rank sum $P = 0.015$). Right, firing rate for projector populations during tones for the reward task alone (alone data: mPFC–BLA $n = 5$ neurons, mPFC–LH $n = 13$ neurons, Wilcoxon rank sum $P = 0.50$; alone versus competition mean *Z* score during tone; mPFC–LH $P = 0.0189$, mPFC–BLA $P = 0.43$). Thicker lines represent the mean. **c**, Left, during reward competition light-off or light-on sessions in which light was delivered in epochs (5-min light epoch of four 5-ms light pulses at 100 Hz every 200 ms). Right, cumulative rewards obtained by ChR2 mice in the light-off versus light-on session ($n = 9$ mice). Data are presented as mean values ± s.e.m. **d**, mPFC–LH cell stimulation increased the number of trials won (left; ChR2 $n = 9$, eYFP $n = 7$; two-way repeated measures ANOVA interaction of virus and light $F_{1,14} = 5.22$, $P = 0.03$; Bonferroni-corrected *t*-test ChR2 $P = 0.01$), time spent occupying the reward port (middle; ChR2 $n = 9$, eYFP $n = 7$; two-way repeated measures ANOVA interaction of virus and light $F_{1,14} = 6.73$, $P = 0.02$; Bonferroni-corrected *t*-test, ChR2 $P = 0.02$) and decreased time spent being displaced (right; ChR2 $n = 9$ paired *t*-test, $P = 0.005$; eYFP $n = 7$ paired *t*-test, $P = 0.28$). *$P < 0.05$, **$P < 0.01$.

while animals were alone versus in social competition (Fig. 3b–d and Extended Data Fig. 9b–d). During competition, but not while alone, relative dominants had more cells that were responsive to self port entries whereas subordinates had larger responses to win trials and port entries of the other (Fig. 3b–d and Extended Data Fig. 9b–d). Furthermore, the mPFC neurons of relative subordinates exhibited larger phasic responses in response to task events, consistent with the longer neural trajectories observed (Fig 2).

mPFC–LH neurons modulate dominance

Given the functional diversity of neural responses from individual mPFC neurons, we next investigated how information was routed out of the mPFC during social competition to downstream subcortical targets.

The lateral hypothalamus (LH) comprises a diversity of cell types and has been shown to drive hypersocial behaviour and social investigation[21], and to modulate social defensive behaviours[22,23]. Further, the LH plays a critical role in energy balance homeostasis[24]—demonstrating the capacity to serve as a homeostatic control centre[25]. On the basis of the conceptual framework for social homeostasis, after social information is detected and evaluated in a rank-dependent manner, it would be sent to a control centre for comparison to a social homeostatic set point[15,26].

We also investigated the mPFC projection to the basolateral amygdala (BLA) because recent evidence suggests that BLA firing rates correlate with the social rank of conspecific faces in non-human primates[27] and the BLA is an important point of convergence for socially derived information[28] to be associated with emotional valence[28–30].

To identify mPFC cells that project monosynaptically to the LH or BLA, we used an intersectional viral strategy to express ChrimsonR in each projection, validated with ex vivo recordings (Fig. 4a and Extended Data Fig. 10a, b). We then wirelessly recorded mPFC neural activity while animals were alone or competing and delivered red light pulses at the end of the competition session to photoidentify mPFC–LH or mPFC–BLA neurons. We found that mPFC–LH neurons had stronger excitation to reward delivery than mPFC–BLA neurons during reward competition, but not when performing the task alone (Fig. 4b and Extended Data Fig. 10c).

Given the selective unmasking of a robust mPFC–LH response to the reward-predictive tone only in the context of social competition (Fig. 4b), we speculated that mPFC–LH neurons could modulate reward-related social competition. To directly test the hypothesis that mPFC–LH neurons have a causal relationship with social-dominance-related behaviour, we expressed either channelrhodopsin 2 (ChR2) or enhanced yellow fluorescent protein (eYFP) in mPFC–LH neurons and implanted an optic fibre in the mPFC (Fig. 4c and Extended Data Fig. 10d). ChR2-expressing mice won more rewards during the entire competition, had greater reward port occupation and spent less time being displaced when they received optical stimulation (Fig. 4d). Stimulating mPFC–LH neurons did not affect reward-seeking behaviour while performing the reward competition assay alone, feeding in the home cage, anxiety, sociability, place preference or general effort (Extended Data Fig. 10e–k).

Conclusion

Together, these data demonstrate that the mPFC neural activity predicts future competitive success, can be decoded to predict both relative and absolute social rank, and uses cortico-hypothalamic circuits to guide social competition behaviour. Development of an ethologically relevant social competition task that incorporates a trial structure allowed us to reveal how related variables updated on different timescales might be parsed and represented separately. Indeed, social rank and competitive success representations occupied orthogonal activity spaces (Fig. 2a), which we speculate is an adaptive strategy that the PFC can use to parse related variables updated on different timescales.

Importantly, the way that mPFC ensembles encode behaviour is dynamic, which suggests a model in which internal states influence how the mPFC modulates behaviour, consistent with a role in flexibly guiding behaviour. Our data demonstrate that cortico-hypothalamic circuits carry social rank information that could potentially modulate the many different neuropeptide- and hormone-expressing subpopulations in the hypothalamus to achieve behavioural modulation. Indeed, we speculate that the mPFC serves as a rank identification node that works in concert with the anterior cingulate cortex to function as a 'detector' to extract signals from social agents and that downstream projections to the hypothalamus may function as the detector node output to a social homeostatic 'control centre', within a purported social homeostatic circuit[15].

This study not only unveils a number of technological advances that together provide a platform for the investigation of social hierarchies, but also begins to integrate pieces of evidence that together support the notion that there is a neural circuit for social homeostasis.

Online content

Any methods, additional references, Nature Research reporting summaries, source data, extended data, supplementary information, acknowledgements, peer review information; details of author contributions and competing interests; and statements of data and code availability are available at https://doi.org/10.1038/s41586-022-04507-5.

1. Chiao, J. Y. Neural basis of social status hierarchy across species. *Curr. Opin. Neurobiol.* **20**, 803–809 (2010).
2. Wang, F., Kessels, H. W. & Hu, H. The mouse that roared: neural mechanisms of social hierarchy. *Trends Neurosci.* **37**, 674–682 (2014).
3. Bernstein, I. S. Dominance: the baby and the bathwater. *Behav. Brain Sci.* **4**, 419–457 (1981).
4. Dewsbury, D. A. Dominance rank, copulatory behavior, and differential reproduction. *Q. Rev. Biol.* **57**, 135–159 (1982).
5. Karamihalev, S. et al. Social dominance mediates behavioral adaptation to chronic stress in a sex-specific manner. *eLife* **9**, e58723 (2020).
6. Hou, X. H. et al. Central control circuit for context-dependent micturition. *Cell* **167**, 73–86 (2016).
7. Zhou, T. et al. History of winning remodels thalamo-PFC circuit to reinforce social dominance. *Science* **357**, 162–168 (2017).
8. Wang, F. et al. Bidirectional control of social hierarchy by synaptic efficacy in medial prefrontal cortex. *Science* **334**, 693–697 (2011).
9. So, N., Franks, B., Lim, S. & Curley, J. P. A social network approach reveals associations between mouse social dominance and brain gene expression. *PLoS ONE* **10**, e0134509 (2015).
10. Zink, C. F. et al. Know your place: neural processing of social hierarchy in humans. *Neuron* **58**, 273–283 (2008).
11. Ligneul, R., Obeso, I., Ruff, C. C. & Dreher, J.-C. Dynamical representation of dominance relationships in the human rostromedial prefrontal cortex. *Curr. Biol.* **26**, 3107–3115 (2016).
12. Miller, E. K. & Cohen, J. D. An integrative theory of prefrontal cortex function. *Annu. Rev. Neurosci.* **24**, 167–202 (2001).
13. Murugan, M. et al. Combined social and spatial coding in a descending projection from the prefrontal cortex. *Cell* **171**, 1663–1677 (2017).
14. Levy, D. R. et al. Dynamics of social representation in the mouse prefrontal cortex. *Nat. Neurosci.* **22**, 2013–2022 (2019).
15. Lee, C. R., Chen, A. & Tye, K. M. The neural circuitry of social homeostasis: consequences of acute versus chronic social isolation. *Cell* **184**, 1500–1516 (2021).
16. Rigotti, M. et al. The importance of mixed selectivity in complex cognitive tasks. *Nature* **497**, 585–590 (2013).
17. Escola, S., Fontanini, A., Katz, D. & Paninski, L. Hidden Markov models for the stimulus-response relationships of multistate neural systems. *Neural Comput.* **23**, 1071–1132 (2011).
18. Calhoun, A. J., Pillow, J. W. & Murthy, M. Unsupervised identification of the internal states that shape natural behavior. *Nat. Neurosci.* **22**, 2040–2049 (2019).
19. Piva, M. et al. The dorsomedial prefrontal cortex computes task-invariant relative subjective value for self and other. *eLife* **8**, e44939 (2019).
20. Dugatkin, L. A. Winner and loser effects and the structure of dominance hierarchies. *Behav. Ecol.* **8**, 583–587 (1997).
21. Nieh, E. H. et al. Inhibitory input from the lateral hypothalamus to the ventral tegmental area disinhibits dopamine neurons and promotes behavioral activation. *Neuron* **90**, 1286–1298 (2016).
22. Rangel, M. J., Baldo, M. V. C., Canteras, N. S. & Hahn, J. D. Evidence of a role for the lateral hypothalamic area juxtadorsomedial region (LHAjd) in defensive behaviors associated with social defeat. *Front. Syst. Neurosci.* **10**, 92 (2016).
23. Li, Y. et al. Hypothalamic circuits for predation and evasion. *Neuron* **97**, 911–924 (2018).
24. Burton, M. J., Rolls, E. T. & Mora, F. Effects of hunger on the responses of neurons in the lateral hypothalamus to the sight and taste of food. *Exp. Neurol.* **51**, 668–677 (1976).
25. Cannon, W. B. Organization for physiological homeostasis. *Physiol. Rev.* **9**, 399–431 (1929).
26. Matthews, G. A. & Tye, K. M. Neural mechanisms of social homeostasis. *Ann. N. Y. Acad. Sci.* **1457**, 5–25 (2019).
27. Munuera, J., Rigotti, M. & Salzman, C. D. Shared neural coding for social hierarchy and reward value in primate amygdala. *Nat. Neurosci.* **21**, 415–423 (2018).
28. Allsop, S. A. et al. Corticoamygdala transfer of socially derived information gates observational learning. *Cell* **173**, 1329–1342 (2018).
29. Felix-Ortiz, A. C., Burgos-Robles, A., Bhagat, N. D., Leppla, C. A. & Tye, K. M. Bidirectional modulation of anxiety-related and social behaviors by amygdala projections to the medial prefrontal cortex. *Neuroscience* **321**, 197–209 (2016).
30. Janak, P. H. & Tye, K. M. From circuits to behaviour in the amygdala. *Nature* **517**, 284–292 (2015).

Reporting summary

Further information on research design is available in the Nature Research Reporting Summary linked to this paper.

Data availability

Source data are provided with this paper. Data will be made available upon reasonable request to the corresponding authors. Source data are provided with this paper.

Code availability

Code for AlphaTracker can be found at https://tyelab.org/tools/ and code for the HMM–GLM model can be found at https://github.com/Tyelab/HMMGLM.

Acknowledgements We thank C. Wildes, R. Revilla Orellano, S. Luo and C. Chang for technical support, A. Calhoun and M. Murthy for useful feedback on our HMM–GLM model and Z. Williams and W. Lee for comments on our manuscript. K.M.T. is an HHMI Investigator and the Wylie Vale Professor at the Salk Institute for Biological Studies, and this work was supported by finance from the JPB Foundation, the Dolby Family Fund, R01-MH115920 (NIMH) and Pioneer Award DP1-AT009925 (NCCIH). N.P.-C. was supported by the Simons Center for the Social Brain, the Ford Foundation, L'Oreal For Women In Science, the Burroughs Wellcome Fund and K99 MH124435-01. C.L. was supported by the AI Institute, SJTU, the Shanghai Qi Zhi Institute, Shanghai Municipal Science and Technology Major Project (2021SHZDZX0102) and the Meta Technology Group.

Author contributions K.M.T., N.P.-C. and K.B. conceptualized the project. N.P.-C. and K.M.T. designed the experiments and supervised all experiments and data analyses. R.W. provided additional supervision of experiments. N.P.-C. wrote the draft of the manuscript. N.P.-C., K.M.T., M.P., R.R.R., F.M., S.M. and K.B. contributed to writing the manuscript and creating the figures. N.P.-C., M.P., J.C.W., R.R.R., S.B.H., R. Patel, M.B., S.M., J.R., D.O.L., R. Pamintuan and H.L. collected and analysed data. K.B. created the HMM–GLM model and assisted with additional machine learning analyses in the manuscript. Z.C. and H.-S.F. created AlphaTracker and assisted in the implementation of tracking and behavioural clustering under the supervision of C.L. R.Z. wrote code and implemented AlphaTracker behavioural clustering. Y.E.Z., L.R.K., F.H.T. and A.B. contributed to data analyses. N.P.-C., K.B., G.A.M., J.P.C., I.R.F., C.L., A.L., R.Z. and K.M.T. made substantial intellectual contributions.

Competing interests The authors declare no competing interests.

Additional information
Supplementary information The online version contains supplementary material available at https://doi.org/10.1038/s41586-022-04507-5.
Correspondence and requests for materials should be addressed to Cewu Lu or Kay M. Tye.
Peer review information *Nature* thanks Steve Chang and the other, anonymous, reviewer(s) for their contribution to the peer review of this work. Peer reviewer reports are available.

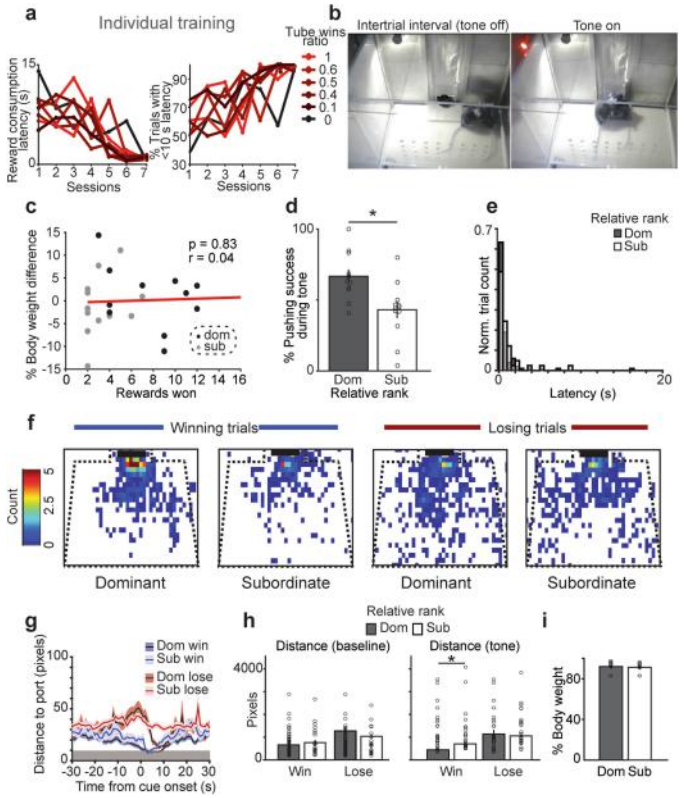

Extended Data Fig. 1 | Additional behavioral metrics during reward competition in unimplanted mice. a, Mice learned the tone reward association at the same rate across social ranks. Left, latency to reward consumption following tone onset decreased over sessions. Right, the percent of trials with a reward consumption latency of less than 10 s increased over sessions (n = 8 mice). Data are plotted as a function of social rank as measured by wins in the tube test. **b**, Example frames from reward competition assay showing intertrial interval time and during the tone period. **c**, Body weight difference between competitors does not correlate with rewards won (n = 12 dyads from 8 mice, Pearson's correlation, p = 0.83). **d**, Relative dominant mice have higher pushing success during the tone (n = 12 per group, paired t-test p = 0.025). **e**, Latency to pick up the reward across trials for relative dominants vs subordinates (*dom*=101, *sub* = 41, Two-sample Kolmogorov-Smirnov test p = 0.29). **f**, Area occupied by dominants or subordinates in the 10 s prior to the tone onset for *win* vs *lose* trials (n = 12 dyads). **g**, Distance to reward port across time by trial type and relative rank (trials n: *dom win*=68, *dom lose* = 24, *sub win* = 24, *sub lose* = 68 from 12 dyads; early baseline −30 to −20 s prior to cue there is no effect of trial nor relative rank; 2-way ANOVA using the mean distance from −5 s to cue onset: main effect of trial type $F_{(1,180)} = 44.4$, $p = 3x10^{-10}$, rank p = 0.94, interaction p=0.09; 2-way ANOVA using the mean distance from 5 s prior to tone until 10 s post tone: main effect of trial type $F_{(1,180)} = 68$, $p = 2.5x10^{-14}$, rank p = 0.071, interaction p = 0.79). Gray rectangle indicates contact range for the reward port. **h**, Total distance traveled immediately before the tone and during the tone period (baseline:10 s prior to tone; tone: 10 s of the tone) across trial types for relative dominant and subordinate mice (*dom win* = 68, *dom lose* = 24, *sub win* = 24, *sub lose* = 68 from 12 dyads; Wilcoxon rank-sum, *baseline win* p = 0.79, *baseline lose* p = 0.59, *tone win* p = 0.028, *tone lose* p = 0.86). Gray zone indicates contact with port. **i**, Percent body weight during food restriction did not differ across relative dominant and subordinate mice (n = 12 dyads, paired t-test, p = 0.23).

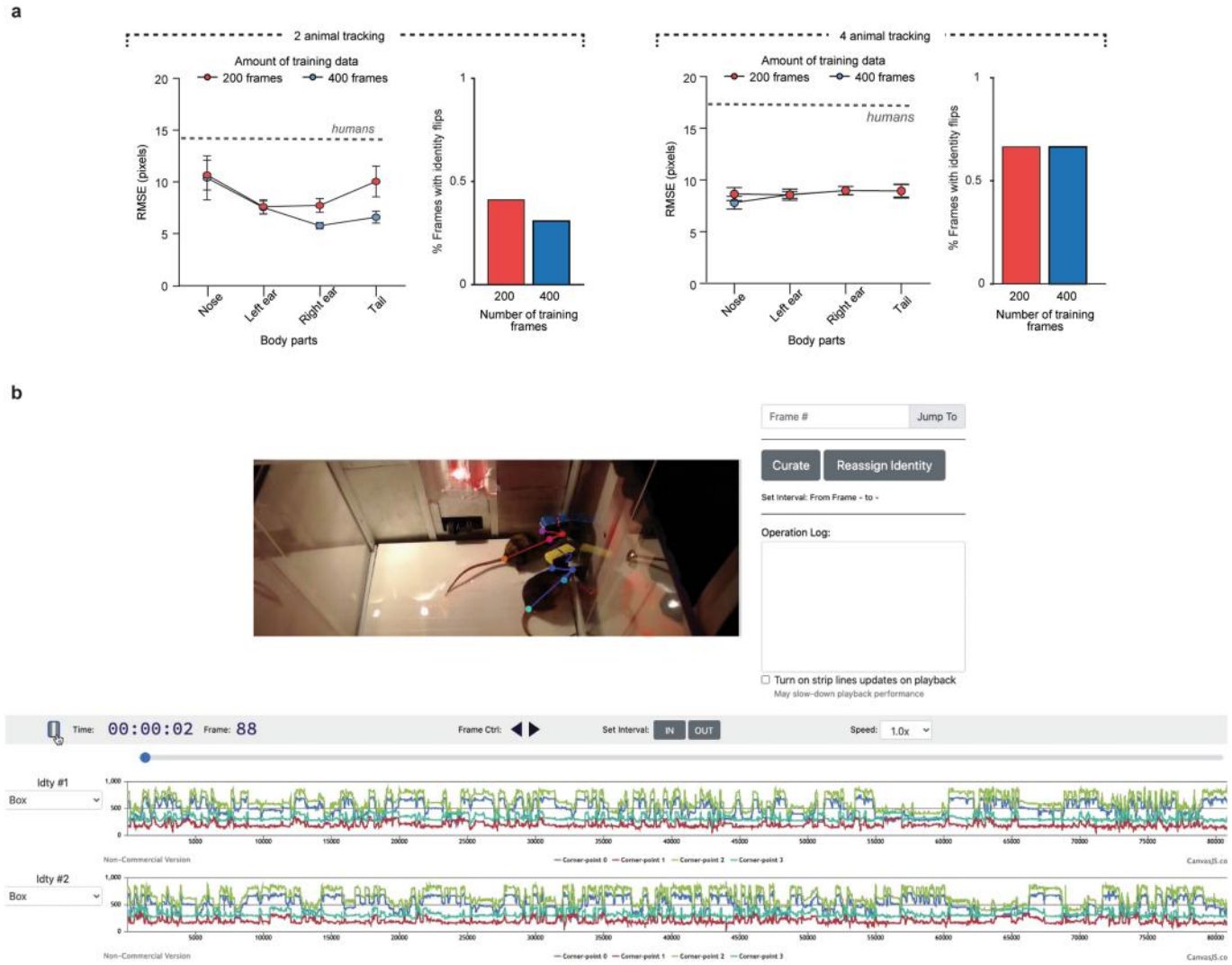

Extended Data Fig. 2 | AlphaTracker tracking metrics. a, Root mean square error (RMSE) and identity error rate of AlphaTracker when tracking different body parts in videos with high resolution (1920x1080 pixels). Left plots have training and tracking done on 2 unmarked mice videos and right plots have training and tracking done on 4 unmarked mice videos. For both datasets two humans annotated the data and the RMSE between humans is indicated with the dashed line. For identity error rate 2 mouse tracking done with 9737 frame video and 4 mouse tracking done with 6020 frame video. **b**, Screenshot of user interface (UI) to fix errors made by AlphaTracker tracking. In addition, this UI can be used for exploring the clustering data.

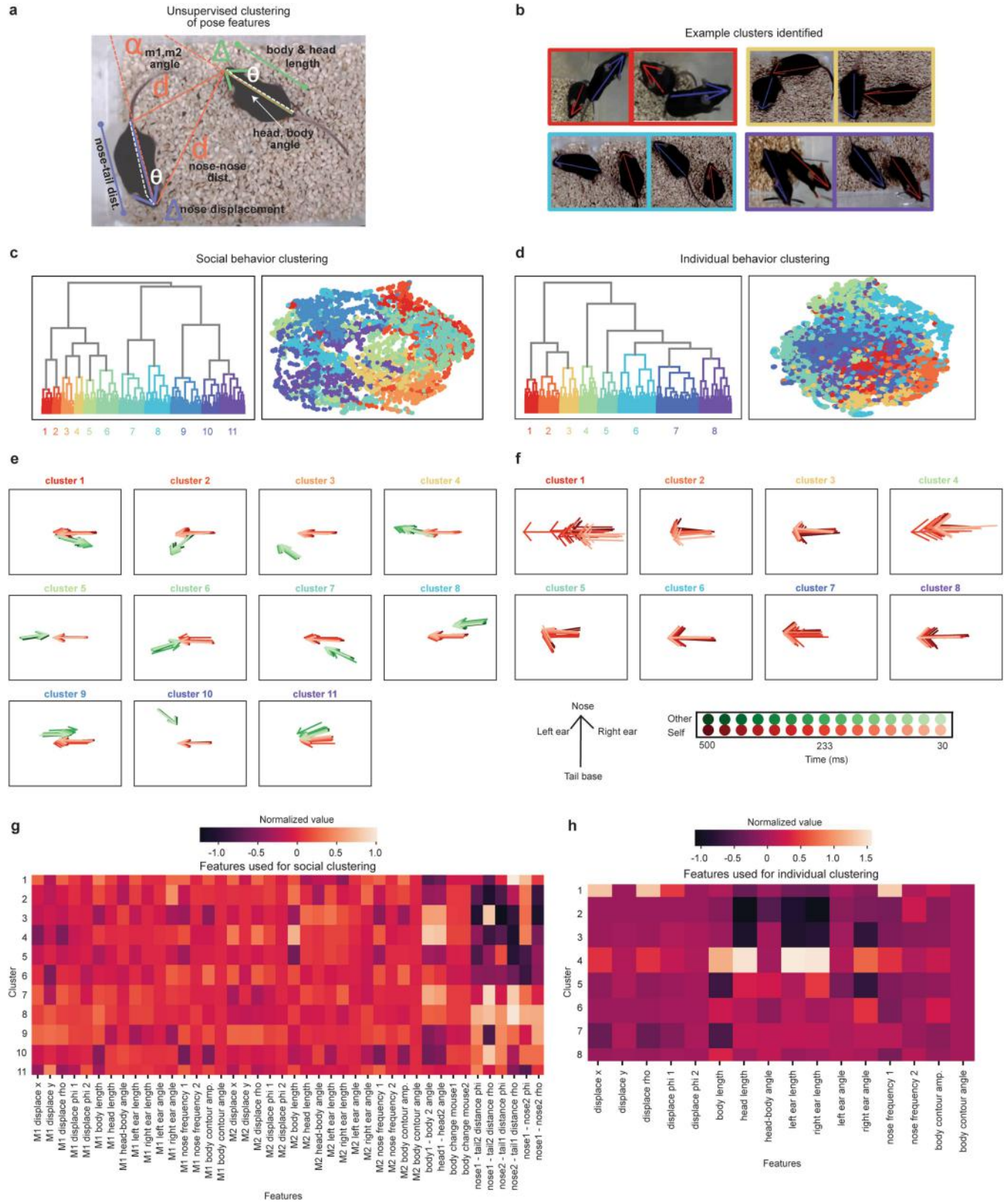

Extended Data Fig. 3 | See next page for caption.

Extended Data Fig. 3 | AlphaTracker unsupervised clustering results. **a**, Diagram depicting features used for AlphaTracker's unsupervised clustering of the tracking datapoints. The features include head length, body length, body-head angle, displacement of the nose, distance between mice, angle between mice. **b**, Example frames from clips belonging to a specific cluster (cluster ID indicated with the color outline in **c**). **c**, Dendrogram and UMAP plot showing all video clips color coded by cluster ID for social behavior clustering. The mean cluster outputs are shown in (**e**) and features used are shown in (**g**). **d**, Dendrogram and UMAP plot showing all video clips color coded by cluster ID for individual behavior clustering. The mean cluster outputs for this clustering are shown in (**f**) and features used are shown in (**h**). **e**, Average normalized skeleton for nose, ears and tail base across clusters for the social behavior clustering across 500 ms of video clip time. Red arrow indicates *self* skeleton and green indicates the *other* skeleton. Each arrow represents 33.3 ms of data (1 frame). **f**, Average normalized skeleton for nose, ears and tail base across clusters for the individual behavior clustering across 500 ms of video clip time. Each arrow represents 33.3 ms of data (1 frame). Legend in bottom applies to panels e-f. **g**, Heatmap of normalized values for the *self* and *other* features used for social behavior clustering. **h**, Heatmap of normalized values for the *self* features used for individual behavior clustering.

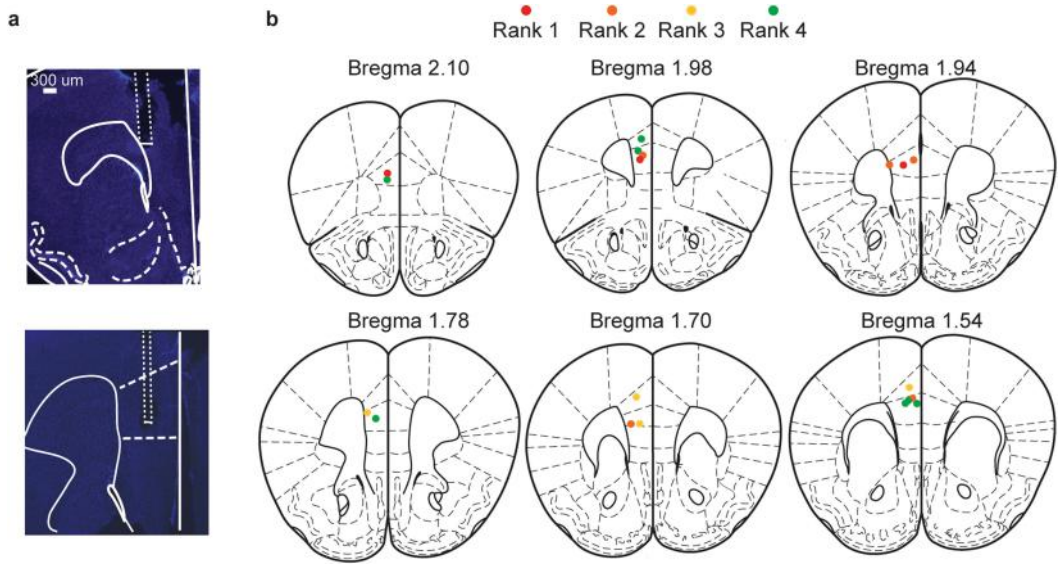

Extended Data Fig. 4 | Histological validation of electrode placements. a, Representative images showing electrode track and lesions of mPFC electrode wires. **b**, Location of center for electrode lesions for all mice color coded by absolute rank across animals.

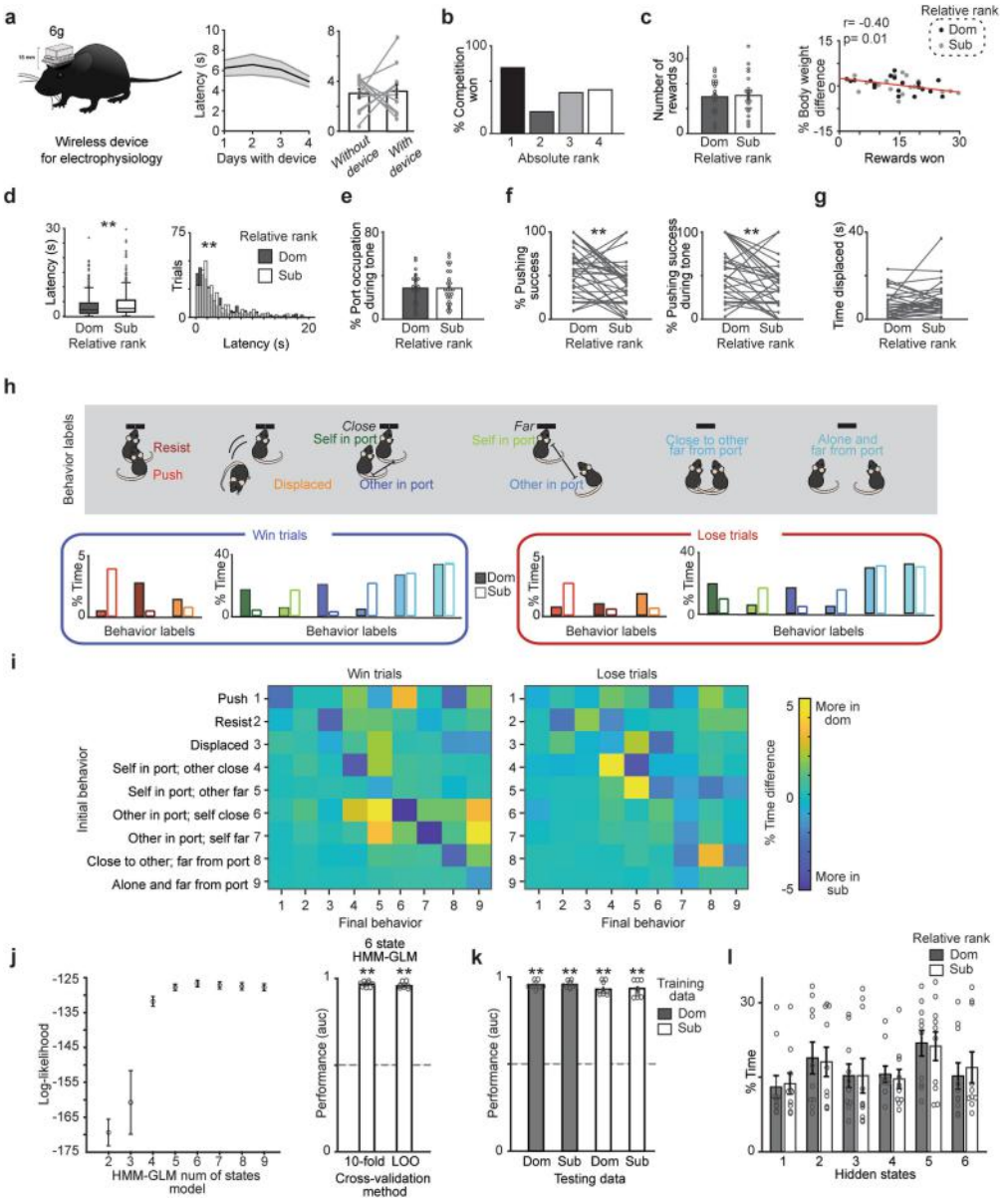

Extended Data Fig. 5 | Behavior in competition with logger and HMM-GLM model controls. a, Left, diagram of wireless electrophysiology recording device used for mPFC recordings. Image modified from SpikeGadgets' MiniLogger product illustration. Middle, latency to collect reward over four days of training (n = 16 mice). Right, latency to collect reward while performing reward task alone was not affected by wearing the logger (n = 12 mice; paired t-test, p = 0.83). **b**, Percent competitions won by absolute rank is highest for rank 1 mice in dataset used for mPFC recordings (number of competitions per rank 1 n = 12; rank 2 n = 12; rank 3 n = 15; rank 4 n = 14). **c**, Left, number of rewards obtained by relative dominants (*dom*) and subordinates (*sub*) during the reward competitions between animals wearing loggers (n = 22 mice per group; paired t-test, p = 0.86). Right, % body weight difference between competitors significantly correlates with rewards won (sub n = 19 dom n = 20, Pearson's correlation, *p = 0.01). For correlation only mice with same day weight measurements were used. **d**, Subordinates had longer latencies to pick up the reward during *win* trials (center line, median; box limits, upper and lower quartiles; whiskers, 1.5x interquartile range; points, outliers). Left, latency per group. Right, histogram of the distribution of latencies across all trials (*dom trials* n = 326, *sub trials* n = 358, Wilcoxon rank-sum, p = 0.012; Two-sample Kolmogorov-Smirnov test, *dom* vs *sub trials* p = 0.015; One way RM-ANOVA $F_{(1,24)} = 2.06$, p = 0.002). **e**, Percent port occupancy during tone across relative rank (n = 31 sessions, paired t-test p = .90). **f**, Relative dominants were more successful displacing subordinates from the reward port throughout the competition (left; n = 32 sessions, paired t-test, p = 0.002) and during the tone time (right; n = 31 sessions, paired t-test, p = 0.005). **g**, Total time being displaced from reward port by relative rank in dataset used for mPFC recordings (n = 31 sessions; paired t-test p = 0.15). **h**, Percent time (normalized by total time per behavior) for 9 behaviors analyzed for *win* and *lose* trials separated by relative social rank. **i**, Percent time difference between relative dominant and subordinates for behavioral transitions during *win* trials (left) vs *lose* trials (right). **j**, Left, model selection for HMM-GLM state number using 10-fold cross-validation method results in a 6 state model being optimal. Error bars indicate standard error across the 10 cross-validations. Right, HMM-GLM 6 state model performance predicts behavioral label regardless of training method utilized (AUC n = 9, one per each behavior label; Sign test of model performance vs chance p = 0.004 for both methods). **k**, HMM-GLM 6 state model predicted behavioral label regardless of which dataset was used for training or testing (n = 9 behavior labels using 482 trials for *dom* vs 478 trials for *sub*; Sign test performance vs 0.5 (chance) p = 0.004 for all tests). **l**, Distribution of percent time spent in each hidden state by relative rank group (n = 10 cross-validations using 482 trials for *dom* vs 478 trials for *sub* from 14 mice).

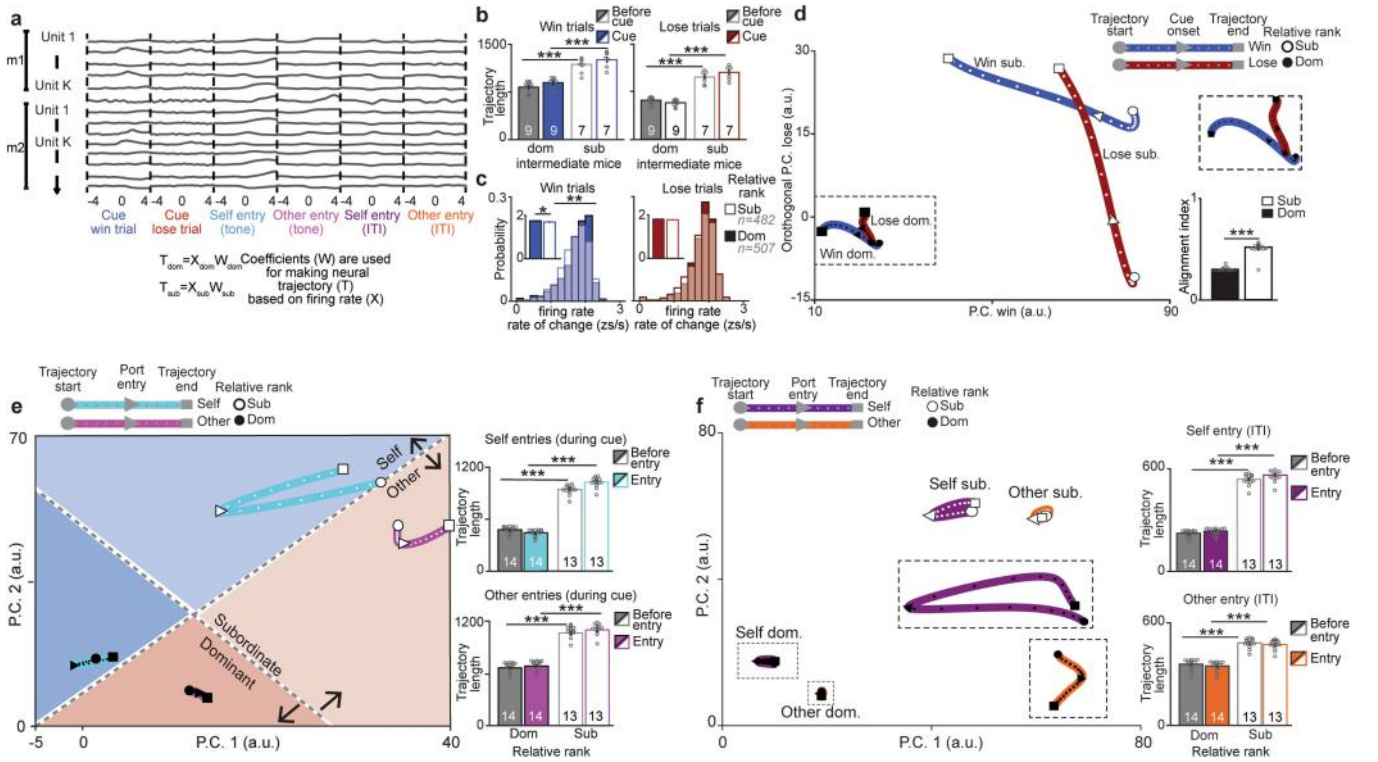

Extended Data Fig. 6 | Additional data for mPFC population dynamics during social competition. a, Data arrangement across all animals (m1 = mouse 1, m2 = mouse 2) for the dimensionality reduction to a common subspace for the six task-relevant events. Neural trajectories were created for dominant and subordinate data using mean firing rate per event and the principal component analysis coefficients. **b**, Neural trajectory lengths (using principal components that captured 90% of variance) for *win* and *lose* trials are longer for relative subordinates in intermediate (ranks 2 or 3) mice (n indicated on plots; *win* 2-way RM-ANOVA main effects of relative rank $F_{(1,14)} = 165$, $p = 2x10^{-6}$; *lose* 2-way RM-ANOVA effect of relative rank $F_{(1,14)} = 262$, $p = 6x10^{-7}$). **c**, Firing rate rate of change is higher for relative dominants only in *win* trials (number of neurons indicated in plots, inset plot has average across groups; *win* trials rate of change: Kolmogorov-Smirnov (KS) test p = 0.009, Wilcoxon rank sum p = 0.01; *lose* trials rate of change: KS test p = 0.40, Wilcoxon rank sum p = 0.19). **d**, Neural trajectories for *win* and *lose* trials plotted in the first Principal Component (PC) for *win* and the orthogonal *lose* subspace show little overlap. Top right, inset of dominant neural trajectories. Bottom right, alignment of *win* and *lose* trajectories was significantly lower for dominant mice (n = 13 per group; Wilcoxon rank-sum, $p = 1.5x10^{-5}$). **e**, Left, neural trajectories of mPFC population firing rate differ by relative rank for port entries that occur during the tone period in a lower dimensional common principal component (PC) *sub*-space (trajectories are the average across leave one out iterations leaving out one mouse at a time, total neurons recorded from dominants: n = 507 and subordinates: n = 490 units from 20 mice). Self entry events are aligned to port entries of the subject mouse while other entry events are aligned to the competitor's port entries. Right, trajectory lengths (using PCs that captured 90% of variance) for *self entry* (top) and *other entry* (bottom) during the tone are longer for relative subordinates (*self entry* 2-way RM-ANOVA effect of relative rank $F_{(1,25)} = 452$, $p = 5x10^{-14}$ and interaction of relative rank and event $F_{(1,25)} = 5,950$, $p = 1x10^{-17}$; *other entry* 2-way ANOVA effect of relative rank $F_{(1,25)} = 728$, $p = 3x10^{-15}$ and interaction of relative rank and event $F_{(1,25)} = 90$, $p = 5x10^{-7}$). **f**, Left, Neural trajectories of mPFC population firing rate for port entries that occur during inter-trial interval (ITI) projected into the first two principal components of the common behavioral subspace. Insets show closer look to the dominant trajectories. Right, neural trajectory lengths for *self entry* (top) and *other entry* (bottom) during the ITI (n = 14 relative dom mice, n = 13 relative sub mice; *self entry*: 2-way RM-ANOVA main effect of rank $F_{(1,25)} = 77.7$, $p = 1x10^{-9}$; *other entry*: 2-way RM-ANOVA main effect of rank $F_{(1,25)} = 110$, $p = 2x10^{-10}$. Self entry events are aligned to port entries of the subject mouse while other entry events are aligned to the competitor's port entries. ITI port entries refer to port entries that occurred outside of the tone period.

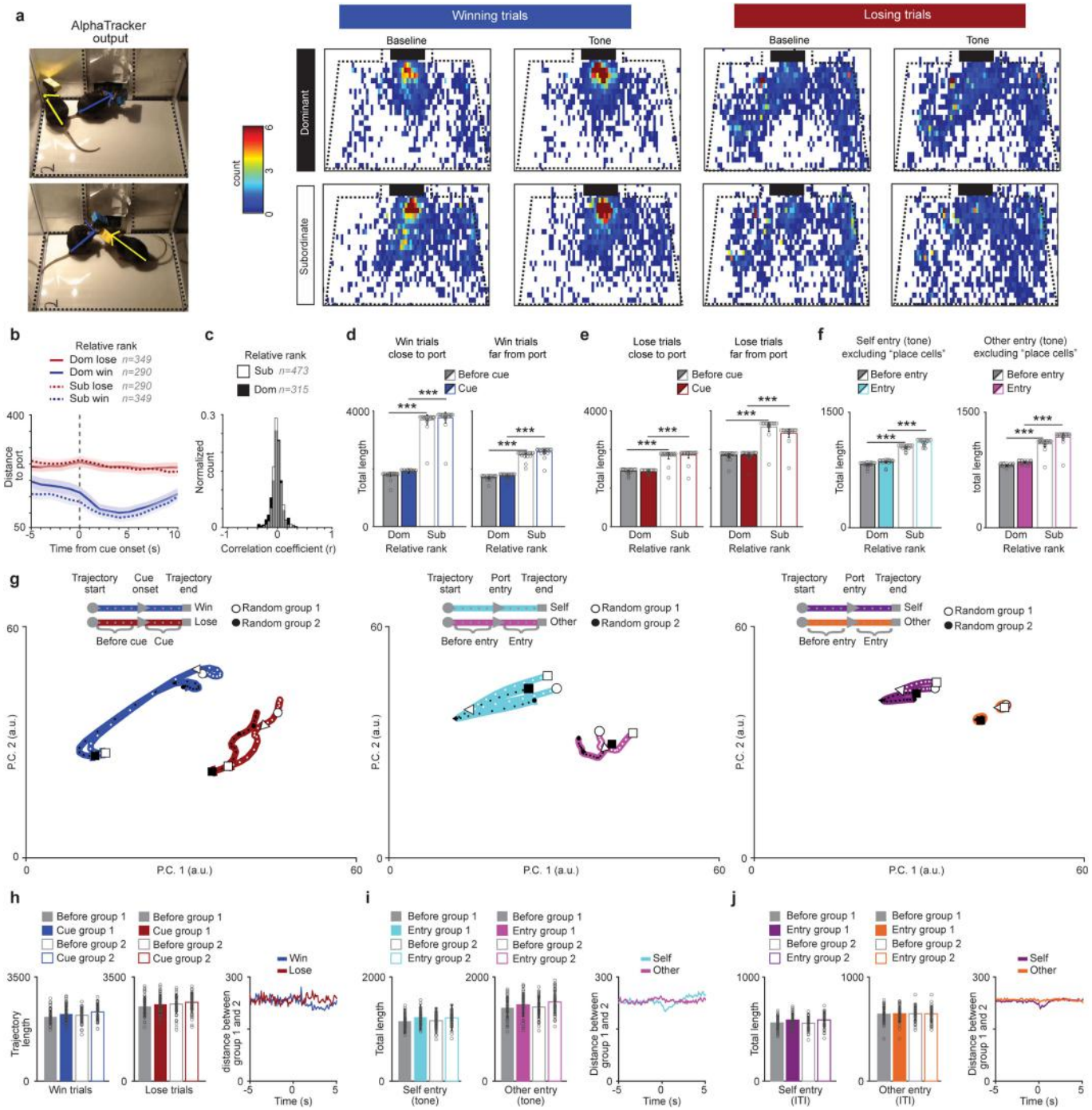

Extended Data Fig. 7 | See next page for caption.

Extended Data Fig. 7 | mPFC population dynamics during social competition are not driven by location or mouse identity. a, Average occupation in different parts of the chamber for *win vs lose* trials for the five seconds prior to tone vs first five seconds of tone. Black squares represent the reward port location. **b**, Distance to reward port differed by trial-type but not by rank (trials: dom win = 290, dom lose = 349, sub win = 349, sub lose = 290; 2-way ANOVA, main effect of trial-type $F(1,1274) = 353$, $p = 8.8x10^{-70}$, rank $p = 0.098$ and interaction $p = 0.066$). **c**, Distribution of the correlation coefficients for firing rate and distance to port for the population of mPFC single units did not differ by rank (dom = 321, sub = 479; KS test, $p = 0.48$). **d**, To determine if distance to reward port affected the population dynamics during *win* and *lose* trials a subset of data with matched video conditions was split by distance to reward port. Neural trajectory lengths were higher for relative subordinates during *win* trials in which mice were close or far to the reward port during tone onset (*dom* n = 19 sessions, *sub* n = 18 sessions; *win close to port*: 2-way RM-ANOVA main effect of rank $F_{(1,35)}=738$, $p = 5x10^{-21}$; *win far from port*: 2-way RM-ANOVA main effect of rank $F_{(1,35)} = 588$, $p=3x10^{-20}$). **e**, Neural trajectory lengths were higher for relative subordinates during *lose* trials in which mice were close or far from reward port during tone onset (*dom* n = 19 sessions, *sub* n = 18 sessions; *lose close to port*: 2-way RM-ANOVA main effect of rank $F_{(1,35)} = 588$, $p = 3x10^{-20}$; *lose far from port*: 2-way RM-ANOVA main effect of rank $F_{(1,35)} = 46.7$, $p = 5x10^{-11}$). **f**, To determine if reward port "place cells" contributed to neural trajectory rank differences we calculated the neural trajectory lengths without cells that were correlated to distance to port in a subset of data with equivalent video settings (video resolution and camera angle). Left, neural trajectories for *self entry* during the tone are highest for relative subordinates without the distance correlated cells (*dom* n = 18 sessions, *sub* n = 18 sessions; 2-way RM-ANOVA main effect of rank $F_{(1,34)} = 94.4$, $p = 1x10^{-13}$). Right, neural trajectories are highest for relative subordinates without the distance correlated cells (*dom* n = 18 sessions, *sub* n = 18 sessions; excluding correlated cells: 2-way RM-ANOVA main effect of rank $F_{(1,34)} = 100$, $p = 1x10^{-13}$). **g**, Neural trajectories of mPFC population activity for two randomly selected halves of the data for (left) *win* and *lose* trials, (middle) port entries during the tone and (right) ITI port entries (data from 49 recording sessions from 20 mice). All trajectories reflect the mean trajectories across 50 bootstrapping iterations. **h**, Left, trajectory lengths for *win* and *lose* trials when data is divided randomly show no effect of group indicating that the effect of rank is not due to chance (n = 50; *win*: 2-way ANOVA, event $F_{(1,196)} = 8.41$, $p = 0.004$, group $p = 0.62$; *lose*: event $p = 0.13$, group $p = 0.65$). Right, mean trajectory distances between groups for *win* and *lose* trials. **i**, Left, trajectory lengths for port entries during the tone when data is divided randomly show no effect of group (n = 50; *self entry*: 2-way ANOVA, event $F_{(1,196)} = 14.2$, $p = 0.0002$, group $p = 0.97$; *other entry*: $F_{(1,196)} = 6.76$, $p = 0.01$, group $p = 0.31$). Right, mean trajectory distances between groups for *self entry* and *other entry* during the tone. **j**, Left, trajectory lengths for ITI port entries when data is divided randomly show no effect of group (n = 50; *self entry*: 2-way ANOVA, event $F_{(1,196)} = 10.3$, $p = 0.001$, group $p = 0.93$; *other entry*: event $p = 0.96$, group $p = 0.87$). Right, mean trajectory distances between groups for *self entry* and *other entry* during the ITI.

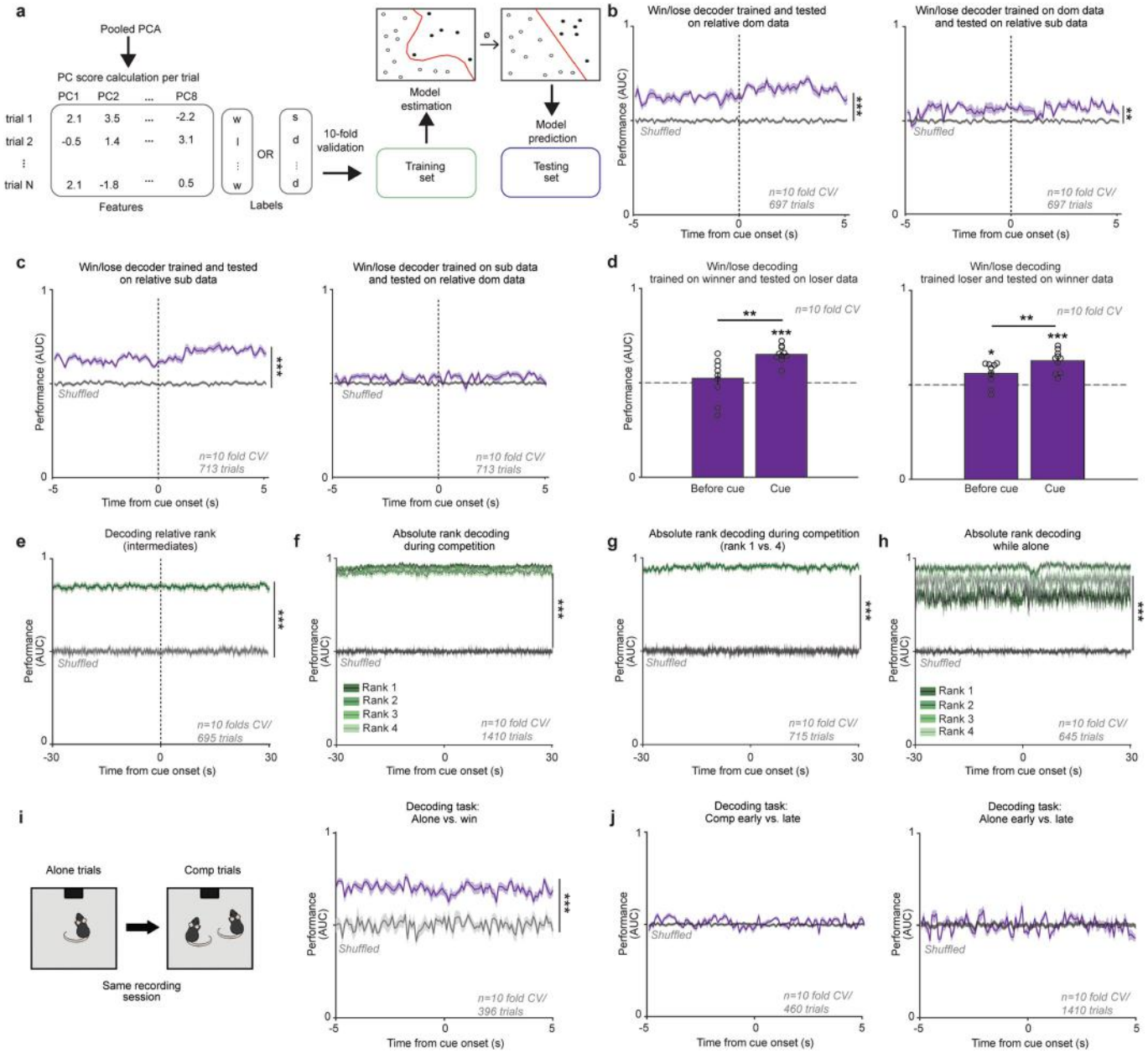

Extended Data Fig. 8 | Decoding performance for relative and absolute social rank, and competitive success with different datasets. a, Support Vector Machine (SVM) data pipeline to decode rank or competition outcome based on single trial population mPFC data in the common behavioral subspace. **b**, mPFC population encoding of win/lose in relative dominants generalizes to relative subordinates. Decoding performance (area under the receiving operating curve; AUC) when (left) training and testing on relative dominant data or (right) training on dominant and tested on relative subordinate data was higher than chance (shuffled performance indicated in gray). (Wilcoxon rank sum, dom/dom p = 0.0002, dom/sub p = 0.003). **c**, mPFC population encoding of win/lose in relative subordinates does not generalize to relative dominants. Decoding performance (area under the receiving operating curve; AUC) when (left) training and testing on relative subordinate data was higher than chance but not when (right) testing on relative dominant data (shuffled performance indicated in gray). (Wilcoxon rank sum, sub/sub p = 0.0002, sub/dom p = 0.14). **d**, Decoder performance for classifying competition outcome using training data from winner data (e.g. mouse won majority of trials) and testing data from loser data (e.g. mouse lost majority of trials) and using training data from loser data and testing data from winner data (Wilcoxon rank sum: left, baseline vs shuffle p = 0.10, left, cue vs shuffle p = 0.0002, right, baseline vs shuffle p = 0.02, right, cue vs shuffle p = 0.0002; Wilcoxon sign rank: loser base vs cue p = 0.002, winner base vs cue p = 0.004). All error bars indicate standard error from 10-fold cross-validation. **e**, SVM performance for decoding relative rank specifically for intermediate (ranks 2 or 3) mice; mean AUC vs shuffled AUC Wilcoxon rank sum: p = 0.0002). **f**, Absolute rank can be decoded from mPFC population activity during social competition. One model was trained per absolute rank (mean performance across ranks vs shuffled data; Wilcoxon rank sum p = 0.0002). **g**, Absolute rank can be decoded for rank 1 and 4 animals from mPFC population activity during social competition. One model was trained to discriminate rank 1 trials from rank 4 (mean performance across ranks vs shuffled data: Wilcoxon rank sum p = 0.0002). **h**, Absolute rank can be decoded from mPFC population activity in mice performing reward task alone. One model was trained per absolute rank (mean performance across ranks vs shuffled data; Wilcoxon rank sum p = 0.0002). **i**, Left, experimental design. In 15 mice the same neurons were recorded during alone trials and followed by competition trials. Right, mPFC population activity can decode between alone tone presentations and win trials during the competition trials (shuffle performance indicated by gray line; mean AUC vs shuffled AUC Wilcoxon rank sum p = 0.0002). **j**, mPFC population activity is not sufficient to decode early vs late trials within task (alone mean AUC vs shuffle AUC Wilcoxon sum rank p = 0.47; comp mean AUC vs shuffle AUC Wilcoxon sum rank p = 0.47).

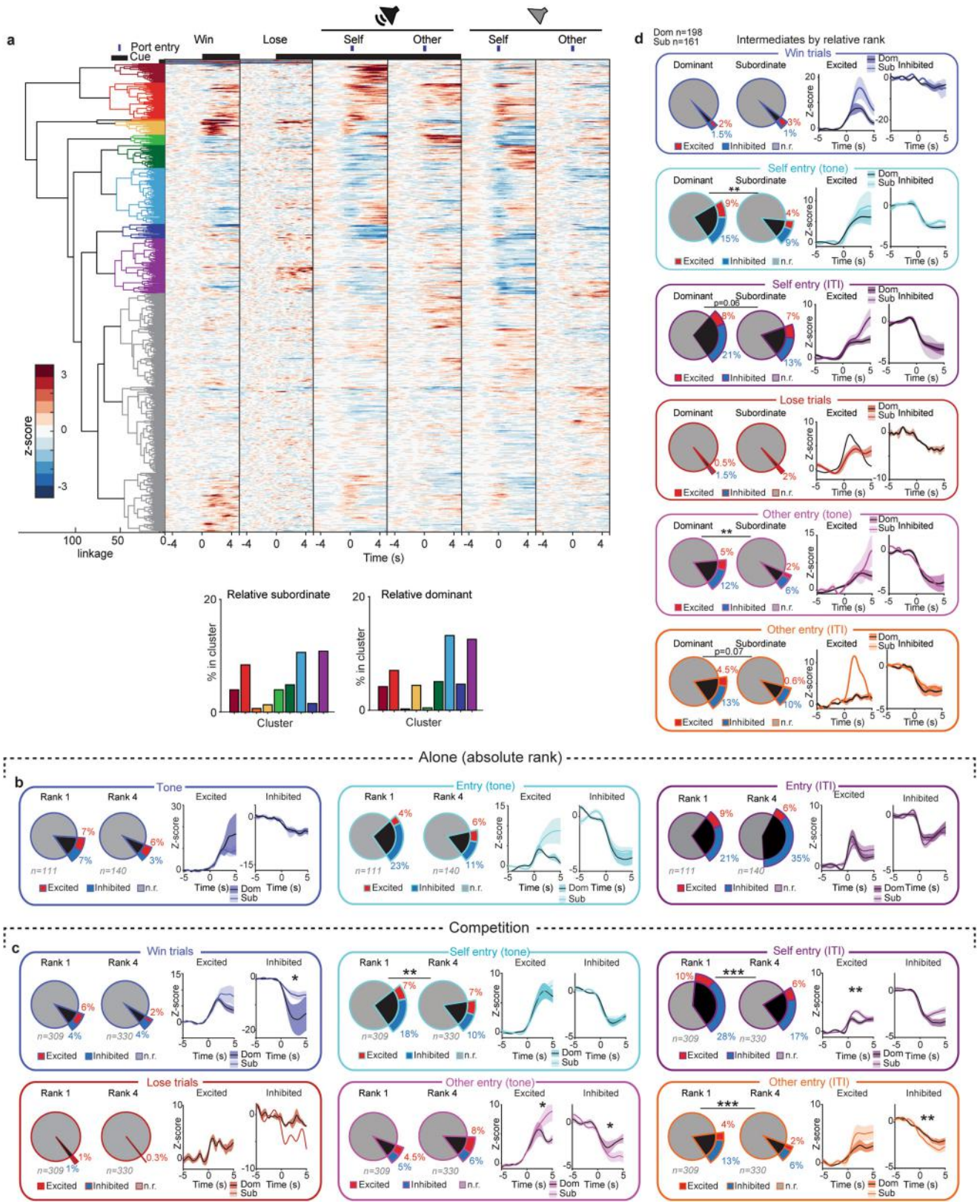

Extended Data Fig. 9 | See next page for caption.

Extended Data Fig. 9 | Additional data for mPFC single unit responses to task-relevant events during social competition. a, Top, Dendrogram for functional clusters and heatmap of mean firing rate for all the neurons included in the hierarchical clustering (n = 913 cells). Gray cells in the dendrogram indicate cells in functional clusters that did not meet criteria of mean z-score being higher than 2 or lower than −1 for at least one event. Bottom, distribution of mPFC cells across functional clusters in relative subordinates and relative dominants. **b**, Left, mPFC tone responsive cells when mice perform the reward task alone. Number of responsive cells and response magnitude to the tone does not differ between rank 1 and rank 4 mice (rank 1 exc = 8 rank 1 inh = 8 rank 4 exc = 8 rank 4 inh = 4; Fisher's exact test, total responsive per group p = 0.16; Wilcoxon rank sum across groups: exc p = 0.87, inh p = 1.0). Middle, mPFC tone *port entries* responsive cells when mice perform the reward task alone. Number of responsive cells and response magnitude to *port entries* during tone does not differ across *dom* (rank 1) vs *sub* (rank 4) mice (*dom* exc = 5 *dom* inh = 25 *sub* exc = 9 *sub* inh = 16; Fisher's exact test, total responsive per group p = 0.09; Wilcoxon rank sum across groups: exc p = 0.23, inh p = 0.62). Right, mPFC inter trial interval (ITI) *port entries* responsive cells when mice perform the reward task alone. Number of responsive cells and response magnitude to *port entries* during ITI does not differ between rank 1 and rank 4 mice (rank 1 exc = 10, rank 1 inh = 23 rank 4 exc = 9 rank 4 inh = 49; Fisher's exact test, total responsive per group p = 0.06; Wilcoxon rank sum across groups: exc p = 0.84, inh p = 0.17). **c**, Total responsive cells and response magnitude to task-relevant event during social competition for absolute rank 1 vs rank 4 (win trials: dom exc = 20, dom inh = 11, sub exc = 7, sub inh = 14, Fisher's exact test p = 0.11, Wilcoxon rank sum exc p = 0.23, inh p = 0.03; lose trials: dom exc = 3 dom inh = 3, sub exc = 0, sub inh = 1, Fisher's exact test p=0.12, Wilcoxon rank sum inh p = 0.50; self entries tone: dom exc = 23, dom inh = 57, sub exc = 24, sub inh=32, Fisher's exact test p = 0.006, Wilcoxon rank sum exc p = 0.42, inh p = 0.77; other entries tone: dom exc=14, dom inh 16, sub exc = 27, sub inh = 19, Fisher's exact test p = 0.11, Wilcoxon rank sum exc p = 0.049, inh p = 0.04; self entries ITI dom exc=31, dom inh = 89, sub exc = 21, sub inh=56, Fisher's exact test p = 2x10-5, Wilcoxon rank sum exc p = 0.01, inh p = 0.41; other entries ITI dom exc=13, dom inh = 41, sub exc = 8, sub inh = 21, Fisher's exact test p = 0.001, Wilcoxon rank sum exc p = 0.11, inh p = 0.008). **d**, Total responsive cells and response magnitude to task-relevant event during social competition for intermediate rank mice (ranks 2 and 3) by relative rank (win trials: dom exc = 4, dom inh = 3, sub exc = 5, sub inh=2, Fisher's exact test p = 0.76, Wilcoxon rank sum exc p = 0.11, inh p = 0.80; lose trials: dom exc = 1 dom inh = 3, sub exc = 3, sub inh = 0, Fisher's exact test p = 1, Wilcoxon rank sum exc p = 1; self entries tone: dom exc = 17, dom inh = 30, sub exc = 7, sub inh = 14, Fisher's exact test p = 0.01, Wilcoxon rank sum exc p = 0.89, inh p = 0.57; other entries tone: dom exc = 10, dom inh 23, sub exc = 3, sub inh = 10, Fisher's exact test p = 0.01, Wilcoxon rank sum exc p = 0.46, inh p = 0.79; self entries ITI dom exc=15, dom inh = 42, sub exc = 11, sub inh = 21, Fisher's exact test p = 0.06, Wilcoxon rank sum exc p = 0.11, inh p = 0.44; other entries ITI dom exc = 9, dom inh = 26, sub exc = 1, sub inh = 16, Fisher's exact test p = 0.07, Wilcoxon rank sum exc p = 0.20, inh p = 0.90).

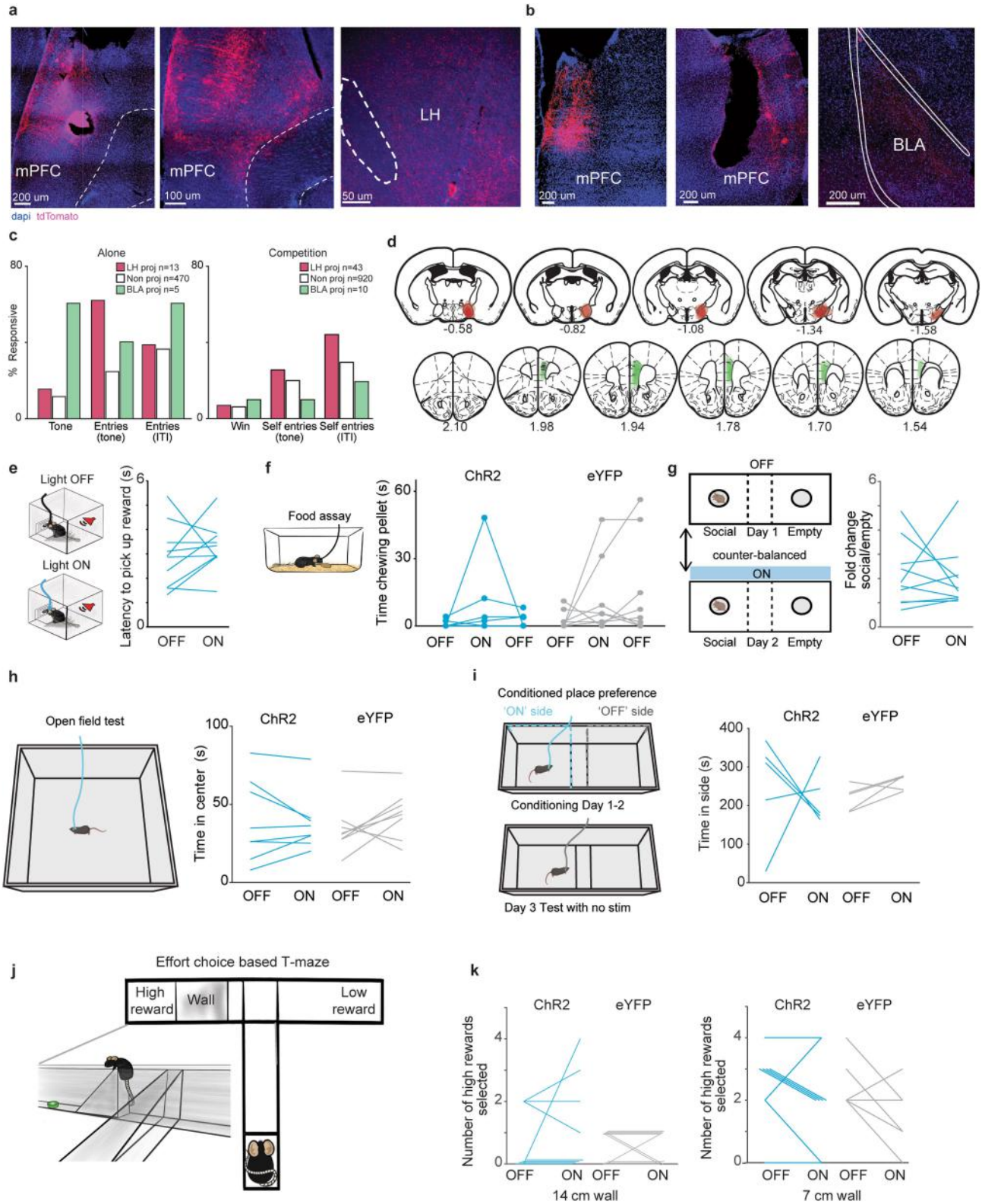

Extended Data Fig. 10 | See next page for caption.

Extended Data Fig. 10 | mPFC-LH photostimulation does not affect other motivated behaviors. a, Representative images showing electrode lesions and mPFC-LH cells and LH axon terminals (tdTomato). **b**, Representative images showing electrode lesions and mPFC-BLA cells and BLA axon terminals (tdTomato). **c**, Responsive cells to tones and port entries while performing the reward task alone vs in social competition (alone: tone mPFC-LH n = 2/13, mPFC-BLA n = 3/5, non-phototagged n = 54/470; entries during tone: mPFC-LH n = 8/13, mPFC-BLA n = 2/5, non-phototagged n = 115/470; entries during ITI: mPFC-LH n = 5/13, mPFC-BLA n = 3/5, non-phototagged n = 170/470; competition win trials: mPFC-LH n = 3/43, mPFC-BLA n = 1/10, non-phototagged n = 62/920; self entries during tone mPFC-LH: n = 11/43, mPFC-BLA n = 1/10, non-phototagged n = 193/920; self entries during ITI: mPFC-LH n = 19/43, mPFC-BLA n = 2/10, non-phototagged n = 271/920, Fisher's exact test non-photo vs LH p = 0.011). **d**, Summary of mPFC optical fiber location (indicated with horizontal gray lines), mPFC viral expression and LH CAV2-Cre injection sites across mice for experiments shown below and in Figure 4. Distance to bregma is indicated under each brain slice. Top row shows LH injection and bottom row shows mPFC injection and fiber. **e**, mPFC-LH photostimulation in ChR2 mice did not change latency to pick reward while performing reward task alone (n = 10; paired t-test, p = 0.42). **f**, mPFC-LH photostimulation did not increase chow eating in the homecage (eYFP n = 8, ChR2 n = 7; 2-way RM ANOVA no significant effect of light, virus or interaction). **g**, mPFC-LH photostimulation in ChR2 mice did not change time spent in social chamber in the 3-chamber social interaction assay (n = 10; paired t-test, p = 0.79). **h**, mPFC-LH photostimulation did not change anxiety-like behavior in the open field (ChR2 n = 8, eYFP n = 8; 2-way repeated measures (RM) ANOVA no significant effect of light, virus or interaction). **i**, mPFC-LH photostimulation did not evoke conditioned placed preference or aversion (ChR2 n = 5, eYFP n = 5; 2-way RM ANOVA no significant effect of light, virus or interaction). **j**, Effort based T-maze allows mice to choose between a low reward low effort arm or a high reward high effort arm in which they must climb a wall to obtain the reward. **k**, mPFC-LH photostimulation did not increase high effort choice in the effort T-maze (ChR2 n = 8, eYFP n = 9; 2-way RM ANOVA no significant effect of light, virus or interaction for both 14 and 7 cm walls).

nature portfolio

Corresponding author(s): Kay M. Tye and Cewu Lu

Last updated by author(s): Nov 13, 2021

Reporting Summary

Nature Portfolio wishes to improve the reproducibility of the work that we publish. This form provides structure for consistency and transparency in reporting. For further information on Nature Portfolio policies, see our Editorial Policies and the Editorial Policy Checklist.

Statistics

For all statistical analyses, confirm that the following items are present in the figure legend, table legend, main text, or Methods section.

n/a	Confirmed
☐	☒ The exact sample size (*n*) for each experimental group/condition, given as a discrete number and unit of measurement
☐	☒ A statement on whether measurements were taken from distinct samples or whether the same sample was measured repeatedly
☐	☒ The statistical test(s) used AND whether they are one- or two-sided *Only common tests should be described solely by name; describe more complex techniques in the Methods section.*
☒	☐ A description of all covariates tested
☐	☒ A description of any assumptions or corrections, such as tests of normality and adjustment for multiple comparisons
☐	☒ A full description of the statistical parameters including central tendency (e.g. means) or other basic estimates (e.g. regression coefficient) AND variation (e.g. standard deviation) or associated estimates of uncertainty (e.g. confidence intervals)
☐	☒ For null hypothesis testing, the test statistic (e.g. *F*, *t*, *r*) with confidence intervals, effect sizes, degrees of freedom and *P* value noted *Give P values as exact values whenever suitable.*
☐	☒ For Bayesian analysis, information on the choice of priors and Markov chain Monte Carlo settings
☐	☒ For hierarchical and complex designs, identification of the appropriate level for tests and full reporting of outcomes
☐	☒ Estimates of effect sizes (e.g. Cohen's *d*, Pearson's *r*), indicating how they were calculated

Our web collection on statistics for biologists contains articles on many of the points above.

Software and code

Policy information about availability of computer code

Data collection	All data were collected with commercially available software reported in the methods. More information is available upon request.
Data analysis	Data were analyzed with commercially available, open-source and custom made code. Descriptions of these analyses are found in the methods. In cases that there are published descriptions of the methods, full references are included. AlphaTracker software is available on github and other custom code is available upon request.

For manuscripts utilizing custom algorithms or software that are central to the research but not yet described in published literature, software must be made available to editors and reviewers. We strongly encourage code deposition in a community repository (e.g. GitHub). See the Nature Portfolio guidelines for submitting code & software for further information.

Data

Policy information about availability of data

All manuscripts must include a data availability statement. This statement should provide the following information, where applicable:

- Accession codes, unique identifiers, or web links for publicly available datasets
- A description of any restrictions on data availability
- For clinical datasets or third party data, please ensure that the statement adheres to our policy

The datasets generated during and/or analyzed during the current study will be made available upon reasonable request.

Field-specific reporting

Please select the one below that is the best fit for your research. If you are not sure, read the appropriate sections before making your selection.

☒ Life sciences ☐ Behavioural & social sciences ☐ Ecological, evolutionary & environmental sciences

For a reference copy of the document with all sections, see nature.com/documents/nr-reporting-summary-flat.pdf

Life sciences study design

All studies must disclose on these points even when the disclosure is negative.

Sample size	Sample sizes were not predetermined and based on similar studies in the literature (Wang et al., 2011; Zhou et al., 2017). Sample size is reported in the legends and methods.
Data exclusions	Subjects with mistargeted viral injections were excluded from analyses. Animals with electrodes that did not had any cells were used as competitors in competition sessions. Electrophysiology recording sessions in which there was battery failures in the recording devices were excluded from the study.
Replication	Our behavioral assay was piloted in a separate group of mice that was not included on this study. In both the pilot and the study we see the same behavioral effects of relative social rank. Our optogenetic experiments were ran in two cohorts and in both we saw the same effect. Many of our neurophysiological findings replicate across different groups of relative rank: using all mice across all ranks, restricting it to intermediate ranks, and looking at just absolute rank 1 vs rank 4 animals.
Randomization	For optogenetic manipulation experiments the cage assignment to control or experimental group was randomized. For behavioral competition experiments and tube testing the order of the competitions was randomized. Given that control recordings with the animals alone were done in the same arena as the competition, all the recording alone controls happened before the competition recordings to avoid context associations of previous competitions during the control recordings. Animals were determined to be relative dominant vs subordinates based on the ranks determined by the tube test which occurred in a randomized order daily for the duration of the experiment.
Blinding	During behavioral testing investigators were not always blind to the animal's ranks given familiarity with the subjects. However, for behavioral scoring the experimenters were blinded to the animal's ranks. For optogenetic experiments the experimenters were blinded to the group assignment of the animals (eYFP vs ChR2). During electrophysiological data processing and analysis experimenters were blinded to the animal's ranks until the point that all data was processed such that group comparisons could be made.

Reporting for specific materials, systems and methods

We require information from authors about some types of materials, experimental systems and methods used in many studies. Here, indicate whether each material, system or method listed is relevant to your study. If you are not sure if a list item applies to your research, read the appropriate section before selecting a response.

Materials & experimental systems

n/a	Involved in the study
☒	☐ Antibodies
☒	☐ Eukaryotic cell lines
☒	☐ Palaeontology and archaeology
☐	☒ Animals and other organisms
☒	☐ Human research participants
☒	☐ Clinical data
☒	☐ Dual use research of concern

Methods

n/a	Involved in the study
☒	☐ ChIP-seq
☒	☐ Flow cytometry
☒	☐ MRI-based neuroimaging

Animals and other organisms

Policy information about studies involving animals; ARRIVE guidelines recommended for reporting animal research

Laboratory animals	Group housed male mice of C57 strain, between the ages of 8-20 weeks were used for all the experiments.
Wild animals	No wild animals were used in this study
Field-collected samples	No field-collected samples were used in this study
Ethics oversight	IACUC Salk Institute for Biological studies and MIT

Note that full information on the approval of the study protocol must also be provided in the manuscript.